CHALMERS
UNIVERSITY OF TECHNOLOGY

Alcohol flexible HD single cylinder diesel engine tests with separate dual high pressure direct fuel injection

Fuel 294 (2021) 120478

Contents lists available at ScienceDirect

Fuel

journal homepage: www.elsevier.com/locate/fuel

Full Length Article

Alcohol flexible HD single cylinder diesel engine tests with separate dual high pressure direct fuel injection

Michael Saccullo *, Andreas Nygren, Timothy Benham, Ingemar Denbratt

Department of Mechanics and Maritime Sciences, Chalmers University of Technology, Göteborg, Sweden

ARTICLE INFO

Keywords:
Dual fuel
Flex fuel engine
Dual direct injection
Heavy duty

ABSTRACT

Both greenhouse gas (GHG) emissions and local emissions from heavy duty (HD) Diesel engines must be greatly reduced to make transportation sustainable and comply with increasingly stringent emissions regulations. The fuel flexible engine concept for HD Diesel engines uses a dual fuel direct injection system in which ignition of the main alcohol fuel, either methanol or ethanol, is induced by a small Diesel pilot injection delivered via a separate direct injector. The objective of this investigation was to find ways to combine the advantages of conventional Diesel engines with the advantages of low carbon fuels and to thereby bypass the soot-NO_x-trade-off. Experiments were conducted using a modified single-cylinder HD engine and three fuels (methanol, ethanol, and a reference Diesel fuel) to determine how the choice of fuel affected the engine's combustion behaviour, emissions and fuel efficiency. Injection pressures on the alcohol side were varied up to 1500 bar and the investigation was carried out at low, medium and high speed-load points. The alcohol fuels significantly outperformed Diesel fuel under all tested conditions (with and without exhaust gas recirculation (EGR)). Indicated thermal efficiency was increased by up to 3.5%-points and simultaneously soot emissions were lowered by a factor of 40 or more and NO_x by 20%. Combustion stability and emissions were in the same range as for Diesel but replacing more than 95 % of the fossil Diesel with an alcohol fuel.

1. Introduction

The demand for transportation has increased significantly in recent decades because of the rising global population, the growing middle class in developing countries, more extensive global trade, and urbanization. Globally, the transportation sector accounts for 17 % of all GHG and also contributes to the increasing incidence of cardiovascular and pulmonary health problems because of its emissions of local pollutants such as NO_x and particulates formed during the combustion of fossil fuels [1,2].

Additionally, there is a global consensus that fossil fuel consumption must be reduced to counter the challenges of global warming, which will have to be primarily achieved by reducing GHG emissions [3]. Consequently, there is a need for new engine technologies that will reduce emissions of harmful pollutants such as NO_x and particulates as well as CO_2. One way to reduce emissions from heavy duty (HD) ICEs is to replace fossil Diesel fuel with low carbon alcohol based-alternatives. Methanol and ethanol have shown particularly promising results in terms of reducing engine out soot emissions while maintaining high combustion efficiencies [4].

Before the use of Diesel particulate filters, Diesel fuel blends with oxygenated fuels were used to reduce particulate and NO_x emissions simultaneously [5,6]. In recent years, considerable effort has been invested into developing low temperature combustion (LTC) concepts that simultaneously reduce soot and NO_x emissions. In LTC, large amounts of EGR are used to cool the combustion process, which increases emissions of unburned hydrocarbons and carbon monoxide (CO) [7–10].

A different approach is to use alternative fuels that have intrinsic advantages in terms of GHG, soot, and NO_x emissions [11]. Fossil Diesel can be replaced with sustainable biofuels, and there is considerable interest in applying this approach in the HD sector [12,13]. Alcohol fuels typically have low cetane numbers and thus exhibit long ignition delays and poor auto-ignitability; this makes them difficult to use as Diesel substitutes under conventional Diesel engine operating conditions [14]. Therefore, dual fuel strategies have been developed using an additional port fuel injection system for the low cetane fuel and direct Diesel injection to facilitate ignition [15]. These strategies can be implemented for various combustion modes and have the potential to reduce both soot

* Corresponding author.
E-mail addresses: michael.saccullo@chalmers.se (M. Saccullo), andreas.nygren@chalmers.se (A. Nygren), benham@chalmers.se (T. Benham), denbratt@chalmers.se (I. Denbratt).

https://doi.org/10.1016/j.fuel.2021.120478
Received 13 May 2020; Received in revised form 3 November 2020; Accepted 10 February 2021
Available online 18 March 2021

Nomenclature

Abbrevations

GHG	Greenhouse Gas Emissions
HD	Heavy Duty
NO_x	Nitrous Oxides
IS…	Indicated specific …
EGR	Exhaust Gas Recirculation
CO_2	Carbon Dioxide
ICE	Internal Combustion Engine
LTC	Low Temperature Combustion
CO	Carbon monoxide
RCCI	Reactivity Controlled Compression Ignition
LHV	Lower Heating Value
CAD	Crank Angle Degrees
TDC	Top Dead Center
SOC	Start of Combustion
$W_{c.ig}$	Gross Indicated Work
$\eta_{f.ig}$	Indicated Thermal Fuel Efficiency
HC	Hydrocarbons
aRoHR	Apparent Rate of Heat Release
CA50	Combustion phasing (50 % of fuel combusted)
CA90	End of Combustion (90 % of fuel combusted)
CFD	Computational Fluid Dynamics
HR	Heat Release
CPV	Combustion Progress Variable
EER	Effective Expansion Ratio
IMEP	Indicated Mean Effective Pressure
COV	Coefficient of Variation
°aTDC	Crank Angle Degrees After Top Dead Center
°bTDC	Crank Angle Degrees Before Top Dead Center
EOI	End of Injection
FSR	Fuel Substitution Ratio

Table 1
Fuel Properties of Diesel, Methanol, and 95 % Ethanol with 5 % water.

	Diesel	Methanol	Ethanol	Unit
Chemical Formula	$C_{10}H_{20}$ to $C_{15}H_{28}$	CH_3OH	C_2H_5OH	
Lower Heating Value[a]	42.87	18.95	23.93	*MJ/kg*
Heat of Vaporization	~ 254	~ 1109	~ 841	*kJ/kg*
Carbon[b]	86.2	36.8	48.3	mass%
Hydrogen[b]	14.3	12.5	13.0	mass%
Oxygen[c]	<0.1	50.7	38.7	mass%

Methods used:[a] ASTM D 240, [b] ASTM D 5291, [c] ASTM D 5291 mod.

emissions and fossil Diesel consumption. A recent review on the use of alcohol-based fuels in Diesel engines by Vallinayagam et al. demonstrates the rising interest in such concepts [16].

1.1. Dual fuel combustion

Dual fuel concepts typically involve port fuel injection of the low reactivity fuel, resulting in largely premixed combustion and controllability problems [17,18]. One way to increase the controllability and responsiveness of a dual fuel engine is to directly inject the low and high cetane fuels into the cylinder. Dual fuel systems based on direct injection of natural gas and Diesel have been investigated by Westport and made commercially available with their high pressure DI (HPDI) of natural gas [19,20]. Fewer investigations have examined this strategy, but an early study by Ullman and Hare using methanol and Diesel in a HD engine yielded promising results [21,22]. Potential advantages aside from the previously mentioned low engine out soot and NO_x emissions include improved fuel efficiency and greater engine flexibility also reported in more recent studies [23]. Wissink et al. used Diesel and gasoline as the high and low cetane fuels in an engine using the direct dual fuel stratification (DDFS) combustion concept [24,25]. This concept was described as a combination of RCCI and partially premixed combustion (PPC) that shares advantages of both strategies.

1.2. Project goals

The injection technique proposed here is similar to DDFS but the combustion strategy is more closely related to that used in conventional Diesel engines, which means that combustion mainly driven by diffusion. A key goal was to minimize the usage of the high cetane fuel (pilot fuel). The study's main objective is to use a dual fuel direct injection

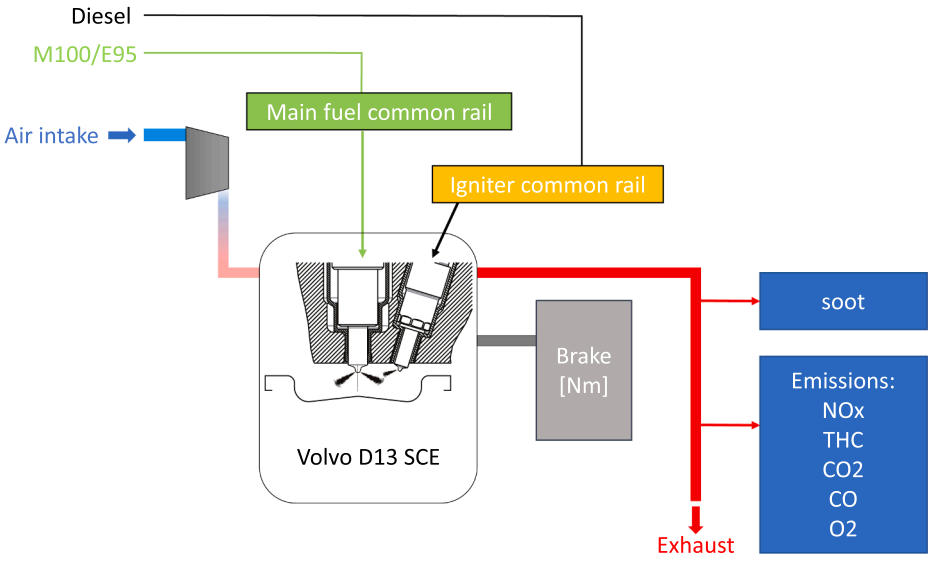

Fig. 1. Experimental set-up of the single cylinder engine test cell.

Table 2
Single cylinder Volvo D13 research engine specifications.

	Value	Unit
Displacement	2.1295	l
Bore	131	mm
Stroke	158	mm
Geometrical Compression Ratio	16.7:1	–

strategy to combine the established advantages of Diesel engines, such as high fuel efficiency [26], with those of alcohol fuels, such as lower particulate and GHG emissions. Engine experiments were conducted to investigate the effects of different alcohol fuels on combustion parameters and patterns, and to relate these effects to engine-out emissions. Fuel efficiencies and indicated emissions were evaluated at different speed-load points, and the results obtained were compared to those achieved using only reference Diesel fuel under the same conditions.

2. Experimental set-up

The experimental set-up and the post-processing of the data are briefly described in this section. A more comprehensive description was presented by Saccullo et. al. [27]. Table 1 specifies the main fuel properties of the three fuels used in this work.

2.1. Single cylinder engine set-up

Fig. 1 is a simplified representation of the experimental set-up including the modified cylinder head and piston bowl shape used in the engine experiments. The test engine has the same specifications as a single cylinder from a standard Volvo D13 6 cylinder engine, which has 460 horsepower and a maximum torque of 2346 Nm. The key parameters of this engine 0 swirl engine are listed in Table 2. The cylinder head was modified to accommodate two injectors instead of one, but keeping all 4 valves, as shown in Fig. 1. The original center-mounted main injector was retained to deliver the main fuel injection, and a light duty passenger car Diesel injector was added, offset from the cylinder center and at a slight angle. The nozzle tip of this second injector projected into the chamber between the two inlet valves. In this paper, the light duty injector is referred to as the side-injector. The spray orientations of the two injectors were adjusted to avoid direct collisions between the sprays. The flow number of the main injector was increased from 2.3 l/min at 100 bar to 4.6 l/min to adjust the injected energy per time unit in order to account for the lower lower heating value (LHV) of methanol; the same injector was used for ethanol. Tests were conducted using a standard Diesel main injector, for reference purposes; Table 4 in the appendix presents the most important features of the injectors used in this investigation. Fuel was supplied to the main and side injectors via separate standard common rail fuel injection systems with separate pump controls.

2.2. Engine control and data acquisition

Fig. 1 shows the different systems needed to control and measure the parameters of interest. Variables studied during this work included the engine speed and torque, exhaust gas composition and temperature, fuel consumption, and in-cylinder engine pressure. The engine speed and torque were measured and recorded using an electric dynamometer that was operated and controlled using AVL Puma open. The Puma system was connected to two AVL 733S/535C fuel conditioning systems that regulated the temperature and pressure of the fuel delivered to the high pressure pumps, and also measured the consumption of the alcohol and Diesel fuels. Engine-specific settings such as the intake and exhaust pressure, intake temperature, and the levels of cooling water and engine oil were also controlled through Puma and set to constant values. The inlet air temperature was kept constant at 30 °C.

An AVL AMA i60 R1C-EGR Exhaust Measurement System was used to measure engine out emissions by downstream sampling of stabilized exhaust gas flows (Table 5). All data recorded in Puma were saved as average values over 2 min and thus represent steady state operation. Soot emissions measurements were performed using an AVL 483 micro soot sensor operated as a standalone system.

An independent system using ATI Vision was set up to control the two common rail fuel injection systems and set the timings, durations, and pressures of each system. The common rail high pressure pumps were driven by externally controlled electric motors operating at constant speeds.

The in-cylinder pressure was measured with an AVL QC34C pressure transducer, with a measurement range from 0 to 250 bar, and recorded with an Osiris fast data acquisition system. This system was also used for high frequency recordings of the injector current pulses of both injectors and the intake temperature and pressure over 100 cycles. The recordings of these variables were resolved in crank angle degrees (CAD) and conducted over the whole cycle, from −360 CAD to 360 CAD (0 CAD being top dead center (TDC)), at a rate of 0.1 deg. According to the engine's design, its thermodynamic loss angle should be between 0.5 and 0.6 CAD before TDC. The thermodynamic loss angle here is defined as the crank angle corresponding to the maximum pressure during a motored case at 1200 rpm.

2.3. Rate meter investigation

A new definition of the start of combustion (SOC) was proposed during the course of a previous investigation on the combustion strategy studied here. This was necessary to investigate the behavior of the fuel injection behavior of the unusually large flow number injector used in the studied engine, and to separate the ignition processes of the pilot and the main fuel, as described by Saccullo et al. [27]. To validate this definition, a separate injection rate measurement campaign was conducted to correlate the injection process of the main fuel with the subsequent heat release. The rate meter tests, which were performed using methanol and ethanol, are briefly described below. The mass flow from main injector was measured using the commercially available Loccioni Mexus 2.0 system. Fuel was injected into a constant volume chamber that was flooded with fuel. The flow rate from the injector could then be determined by measuring the pressure rise inside the chamber. The flow was also measured downstream of the constant volume chamber using a Coriolis meter. The same common rail system and the large flow number injector as in the single cylinder tests were used during these experiments.

2.4. Data post-processing

Two different sets of data were created for each measurement point: fast data collected using the Osiris system and slow data collected using the Puma system. A Savitsky-Golay low pass filter was applied to the raw in-cylinder pressure signal to remove unwanted noise. The window length was set to 5 CAD and a polynomial fit of 4 was applied. Those values gave the best results in terms of filtering noise without obscuring physical phenomena occurring during the combustion process [28].

All calculations were performed on a gross indicated basis, meaning that only the compression and expansion strokes were considered, also called close cycle. This was done to facilitate comparisons with previously reported experimental results. Equations for the gross indicated work $W_{c,ig}$ and indicated thermal fuel efficiency $\eta_{f,ig}$ were taken from Heywood [26]. The $W_{c,ig}$ was also used to derive the indicated engine out emissions of NO_x, CO_2, soot, total hydrocarbons (*HC*), and carbon monoxide (*CO*). The combination of methanol and Diesel fuel is henceforth referred to as methanol. The combination of ethanol and Diesel fuel is referred to as ethanol, and the neat reference Diesel fuel is referred to as Diesel.

Table 3
Engine test speed-load points.

Point	Speed [rpm]	Torque [Nm]
Low speed and load	871	86
Medium speed and load	1262	172
High speed 75% load	1508	285

2.4.1. Heat Release analysis

Apparent rate of heat release (*aRoHR*) calculations are commonly performed to investigate and compare combustion processes in internal combustion engines. Apparent in this case means that heat transfer to the combustion chamber walls (cylinder head, liner, and piston) is not modelled. Despite this limitation, such calculations are important tools for in-depth studies on combustion processes and associated phenomena [29]. The expression used to compute the heat release rate is derived from the first law of thermodynamics and is well described by Heywood [26]. Heat release calculations were performed based on mean pressure traces.

Several important parameters can be derived from the heat release rate. Among these is the combustion phasing, or *CA*50, i.e. the crank angle at which 50% of the fuel has combusted. The *CA*50 value is a good indicator of the positioning of the combustion process and is a very useful quantity for comparing different fuels in the same test engine, especially when considered together with the combustion duration [30,31]. The combustion duration is often defined as the length of time between *CA*10 and *CA*90. However, in this work it is defined as the length of time between *SOC* and *CA*90, which is not the same.

2.4.2. CFD simulations

CFD simulations were conducted in order to visualize and interpret significant events on the HR curves. Those simulations are part of another investigation, but shall support the authors discussion points. The CFD simulations were made using the open source CFD toolbox OpenFOAM-2.2.x on a grid containing 383 949 cells at TDC, representing the full geometry during the closed part of the cycle. To account for the piston motion, dynamic mesh layering is used as described by Luccini et.al. [32]. The spray injections was modeled using the VSB2 spray model, which uses the Eulerian–Lagrangian approach to model the spray formation [33]. To model the combustion process, and the evolution of chemical species, a proprietary multi-fuel chemical mechanism that includes 386 species and 2343 reactions were used [34]. To reduce the computational time, the combustion progress variable (CPV) model was used by coupling the external library LOGE-CPV to OpenFOAM [35]. This greatly reduces computational time by utilizing a pre-tabulated version of the chemical mechanism.

3. Results and Discussion

This section presents and discusses the findings of the experimental campaign. Each of the three speed-load points is discussed separately, and the discussions are divided into two parts. The first compares the aRoHR of the different alcohol fuels and the reference Diesel. Special focus is placed on the different phases of the combustion process and on comprehensively describing the combustion patterns observed with this experimental set-up at the same combustion phasing. The phasings for each speed-load case differed slightly but were between 7 and 9 °aTDC, which was reported as the optimum for almost all engines [30]. The second part deals with combustion parameters and engine out emissions. Variables considered in this part include combustion parameters such as $\eta_{f,ig}$, the start of combustion, combustion duration, the coefficient of variation (COV) in IMEP, effective expansion ratio (EER), and engine out emissions of NO_x, CO_2, CO, soot, and *HC*. The relevant chemical properties of each fuel, presented in Table 1 are used to calculate certain quantities (see the appendix for details). Table 3 presents the three constant speed-load points considered in this work. All experiments were performed under steady-state conditions. Each speed-load point represents a distinct area from the engine map of a typical long haul truck. 871 rpm and 86 Nm is a point at low vehicle speed and 1262 rpm and 172 Nm representing a motorway cruising vehicle speed. An elaborate investigation at full load was not possible because the peak pressure of the test engine could not exceed 200 bar. A speed-load point of 1508 rpm and 285 Nm was therefore used to represent high speed-load operation.

The aRoHR curves, emissions, and combustion parameters observed when using methanol, ethanol, and Diesel are presented in the same fashion for each of three speed-load points listed in Table 3 (with and without EGR). The combustion process was divided into the following 5 phases, each of which can be distinguished in the heat release curves:

- **Phase 1:** Heat release of the Diesel pilot and followed by ignition of the main fuel
- **Phase 2:** Premixed combustion of the main fuel and followed by free-flame combustion
- **Phase 3:** Flame-wall interaction between the combusting main fuel and the piston bowl
- **Phase 4:** Flame-flame interaction between adjacent sprays leading to formation of the radial mixing zone (RMZ), and HR after EOI
- **Phase 5:** Heat release tail and late cycle oxidation

The main results are presented using figures whose structure is described below. The first speed-load case is described more extensively than the others because they have many similarities. However, unique phenomena observed in each case are discussed in detail. The aRoHR traces for all three fuels are shown for each case. The heat release rate plots also show the recorded current signals driving the two injectors at the bottom of each sub-figure; the dotted pulses represent the pilot injection event and the solid lines represent the main injection event. The dwell time between the pilot and main injections was kept constant at 3 *CAD*, and the pilot injection pressure was 500 bar. A pilot duration of 0.4 ms was found to be sufficient to induce ignition of the alcohol fuels and was therefore used in all experiments presented here. The heat release signal generated by the pilot was small but clearly visible in all cases.

A main fuel injection pressure of 1250 bar was used in all cases to maintain comparable conditions in terms of turbulence and fuel–air mixing. The plots without *EGR* contain an additional dash-dotted curve showing results obtained using ethanol with an injection pressure of 1000 bar. This slightly lower ethanol injection pressure was used to study the aRoHR at the same injected energy per *CAD* as for Diesel and methanol. This was necessary because the injector nozzle flow value was adjusted to account for the lower *LHV* of methanol compared to Diesel, and the same nozzle was used in the tests with ethanol. However, the *LHV* of ethanol is about 25 % greater than that of methanol, so when the injection pressures for the two fuels are identical, the injected energy per *CAD* is higher for ethanol than for methanol. Equalizing the rate of energy injection for methanol and ethanol is important when comparing the effects of different operating conditions and when considering the influence of *EGR*. Three additional graphs show selected emissions for each case at constant injection pressure (on the left), key combustion parameters (in the middle), and engine performance variables including the fuel efficiency, the effective expansion ratio (EER), and the COV_{IMEP} (on the right). The EER is a way to describe the placement of the heat release curve well described by Stanton [30]. A larger value for the EER means that the combustion of during the closed cycle occurs during its thermodynamically favorable position. A lower value explains a lower closed cycle efficiency. The COV_{IMEP} quantifies the variability of the indicated work per cycle in terms of the standard deviation of the indicated mean effective pressure (*IMEP*), expressed as a percentage. The *CoV* was generally smaller than 1 % and never exceeded 2 %. The figures also show error bars whose lengths are equal to the first standard deviation, which was determined by duplicating each experiment for each speed-load point and fuel. The error bars are generally small,

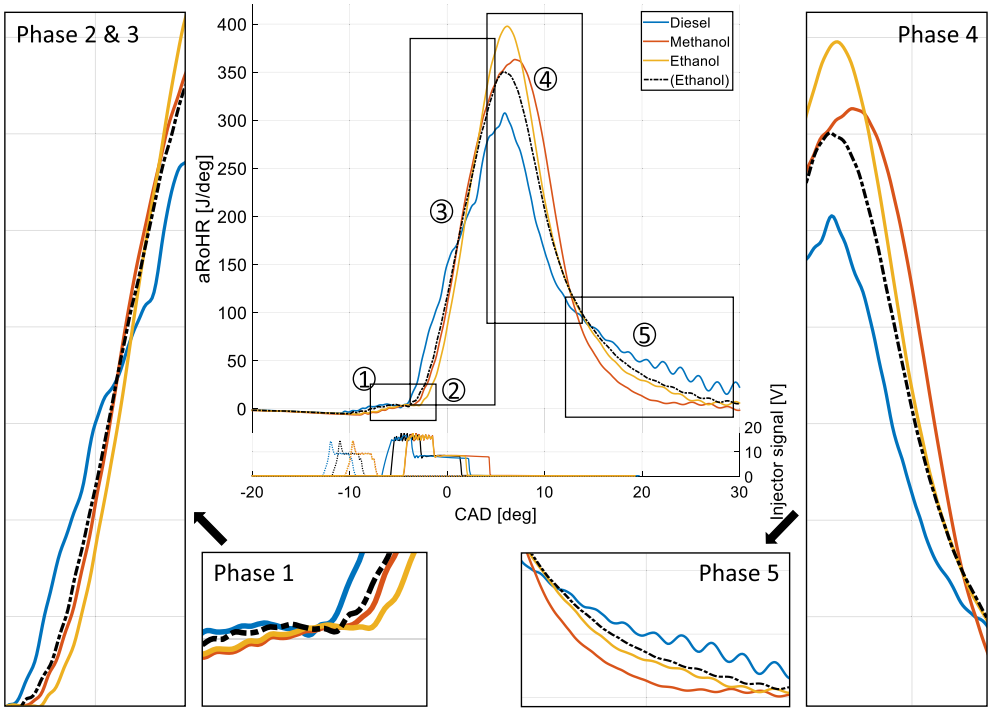

Fig. 2. Apparent rate of heat release curves for Diesel, methanol and ethanol at the 1262 rpm and 172 Nm speed-load point, highlighting 5 important phases of the combustion process.

indicating stable operating conditions and minimal problems with data collection.

The trends observed for ethanol when the rate of energy injection was equal to that for methanol and Diesel did not differ significantly from those observed without equalizing the rate of energy injection. The main settings and results for all cases are presented in the appendix.

3.1. Comparison of methanol and ethanol dual fuel combustion to neat Diesel

This subsection directly compares 6 different aRoHR curves for methanol, ethanol, and the reference Diesel fuel at each of the 3 speed-load points, with and without 20 % EGR. The analysis is based on pairwise comparisons at the same speed-load point. Each case is discussed in its own sub-subsection.

3.1.1. aRoHR at 1262 rpm and 172 nm

The intermediate speed-load point (1262 rpm and 172 Nm) was investigated first; the resulting aRoHR curves are shown in Fig. 2. Fig. 4a shows the pressure traces recorded to calculate the aRoHR curves. The discussions and explanations were derived from the aRoHR curves and the pressure traces for the other cases are therefore not depicted. Peak pressure values can be found in the appendix. Engine settings were kept constant, and the injection duration and timing were adjusted slightly to achieve the desired torque and combustion phasing of about 7 °aTDC at the given engine speed. This phasing causes the main part of the combustion to occur under the most thermodynamically favorable conditions, resulting in a good trade-off for thermodynamic efficiency [26].

Fig. 2 compares the heat release curves for methanol, ethanol, and Diesel. Expansions showing each phase of the combustion process separately are presented to facilitate understanding.

Phase 1 corresponds to the combustion of the Diesel pilot. This results in a small increase in the heat release rate that is very similar for all fuels. The injection of the main fuel causes a small reduction in the heat release rate due to the initial evaporation of the fuel. The ignition delay is very short, as demonstrated by the immediate increase in the heat release rate visible in Fig. 3. This figure shows the apparent heat release rate and the mass flow from the injector as functions of the crank angle, together with the injector trigger signals recorded by the rate meter and in the engine test cell in the bottom. On top there it shows 3D stoichiometric surfcae plots of the combusting main fuel during the injection calculated as CFD simulations of this particular case. The good agreement between these two signals indicates that the injection events in the rate meter and engine test cell are comparable. The injection pressure and duration were identical to the duration at this speed-load point. It has been reported that an in-cylinder temperature of 1100 K is needed to achieve reliable ignition of methanol and ethanol. The results obtained for the pilot show that it consistently created a high enough local temperature to induce ignition of the alcohols in each cycle. Additionally, the pressure rise rates under these conditions did not exceed the normal range for the studied engine at the intermediate speed-load point, which strongly suggests that the environment was hot enough for ignition to occur as intended [14]. All fuels were injected into almost identical environments, so the results obtained for each fuel can be compared directly. For the most part, the combustion of the main fuel occurred in diffusion controlled mode, and the conceptual Diesel flame and air-mixing model developed by Dec appeared to be appropriate for both methanol and ethanol [36].

Phase 2 starts with the premixed combustion phase and is proceeded by the free-flame jet propagating from the nozzle towards the piston bowl. This phase ends when the fuel combustion speed falls significantly near the peak of the heat release curve; this occurs when the flame jet impinges on the piston bowl walls, slowing the combustion process. All three fuels have a very short premixed combustion phases during which the initially evaporated air–fuel mixture burns. After the premixed phase, the slope of the alcohol curves is clearly steeper than that for Diesel, indicating faster combustion. Ethanol combusts slightly faster than methanol, which can be attributed to its greater *LHV*; a higher *LHV* results in a more rapid input of chemical energy at a given injection rate. When the injection pressure of ethanol was reduced to equalize the rate of injection of chemical energy with that for methanol, the initial burning velocities of the two fuels were very similar. Otherwise, the

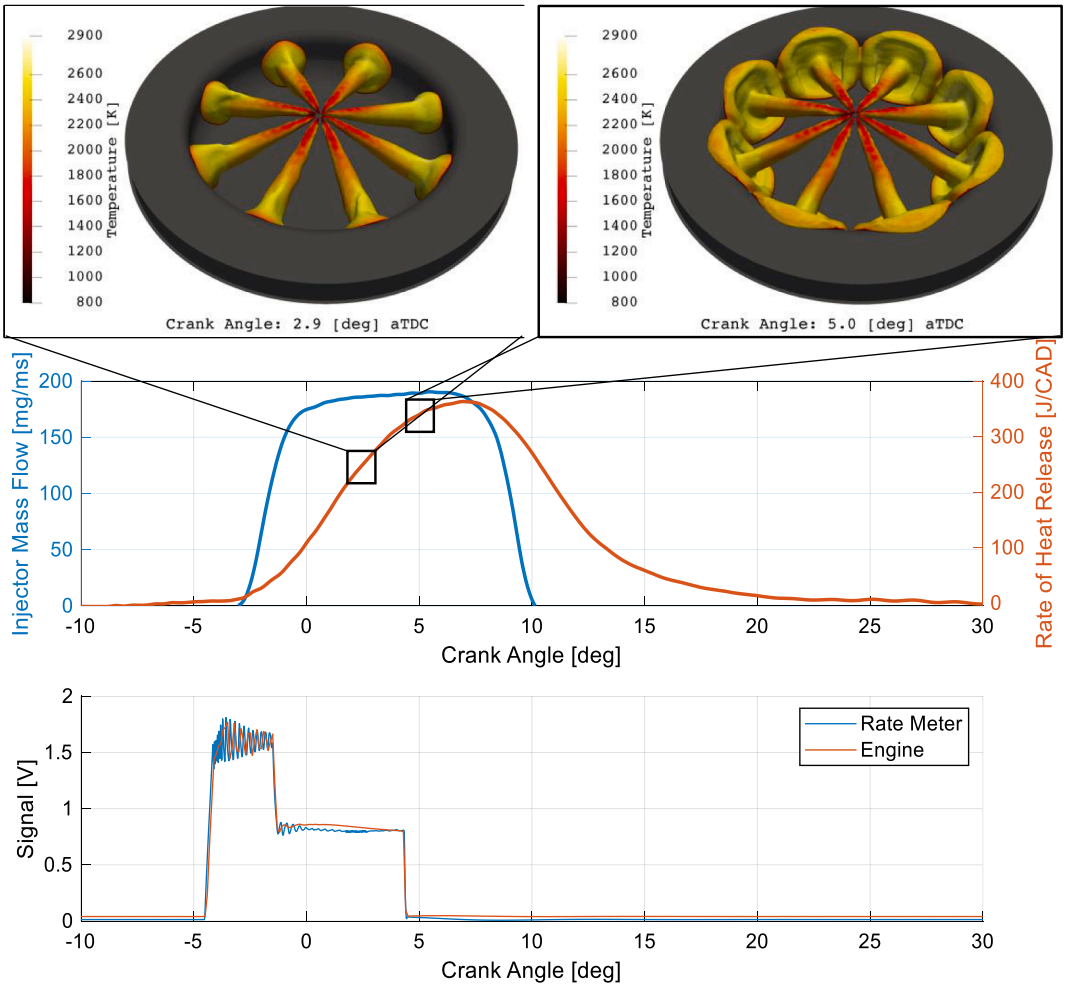

Fig. 3. Top: Preliminary CFD results showing flame-wall and flame-flame interactions at 1262 RPM 172 Nm. Middle: Interpolated injection rates and aRoHR curves for the studied fuels with an injection duration of 1172 μs. Bottom: The injector trigger signals recorded by the rate meter and in the engine test cell.

alcohol curves appear very similar in this phase. The differences in combustion speed between Diesel and the alcohol fuels can partially be explained by the differences in the fuels' chemical composition (unlike Diesel, the alcohols contain oxygen, which facilitates combustion), the mass of fuel injected, and the number and diameter of nozzle holes. The mass of alcohol injected per *CAD* is greater than that of Diesel, creating a higher level of in-cylinder turbulence; this enhances fuel–air mixing and thus increases the speed of the combustion. For Diesel, the premixed combustion phase ends at around 4 °aTDC and 280 J/deg. The curves for the alcohols do not slow at the same rate - the expansion of the HR curves shown in Fig. 3 show that methanol combustion began to slow at around 3 °aTDC and 290 J/deg while ethanol combustion began to slow at around 3.5 °aTDC and 360 J/deg.

Phase 3 is the flame-wall interaction phase in which the flame front meets the piston bowl wall and is forced to deviate from the initial spray direction; it subsequently mainly moves inside the piston bowl. This point can be identified by a decrease in the slope of the *aRoHR* curve caused by a deceleration of the combustion process due to reductions in the flame surface area and the turbulent kinetic energy. However, the rate of heat release continues increasing. The exact point at which the free flame hits the piston bowl wall is difficult to identify in the *HR* curves of the alcohol fuels, but *CFD* calculations (see Fig. 3) do show the initial flame-wall interaction and support the suggested location of this event on the *HR* curve.

During Phase 4, the flames from the different sprays meet and flame-flame interaction zones emerge around the peaks of each fuel. Previous studies suggest that combustion slows down when two flame fronts collide because of the reduced oxygen content in the flames, especially after the formation of the radial mixing zone discussed by Eismark et. al. This point is clearly visible in both the aRoHR curves at around 5 °aTDC and in the CFD image shown in Fig. 3. When using Diesel as the fuel, the deceleration of combustion was followed by a sharp increase in heat release towards the peak (310 J/deg). This was probably a consequence of the experimental setup: the piston dome was lowered to prevent the pilot spray from colliding with it and risking poor ignition of the main fuel. While the shape of the Diesel heat release curve observed here differs somewhat from previously reported curves, this difference does not affect the main findings of this work because all three fuels were tested using the same setup. However, the heat release rate peak for Diesel was significantly lower than those for methanol (370 J/deg) and ethanol (almost 400 J/deg), due to the significantly greater combustion speed. Injecting ethanol at a lower injection pressure to equalize the rate of energy injection with that of methanol reduced the peak heat release rate to 350 J/deg, which is slightly below that for methanol. The peak is followed by a steep decrease in the rate of heat release caused by the end of the fuel injection (*EOI*) event. Methanol exhibited the steepest decrease in the heat release rate after *EOI*, followed by ethanol and Diesel.

During this phase, the radial mixing zone is formed by side vortices created by the redirection of the flames after their interaction with the piston bowl. In this zone, fuel-rich pockets can form; together with the comparatively low combustion temperature, this can cause soot formation later in phase 5 (late cycle oxidation). The combustion tail is shortest for methanol, followed by ethanol, and Diesel. The tails of both

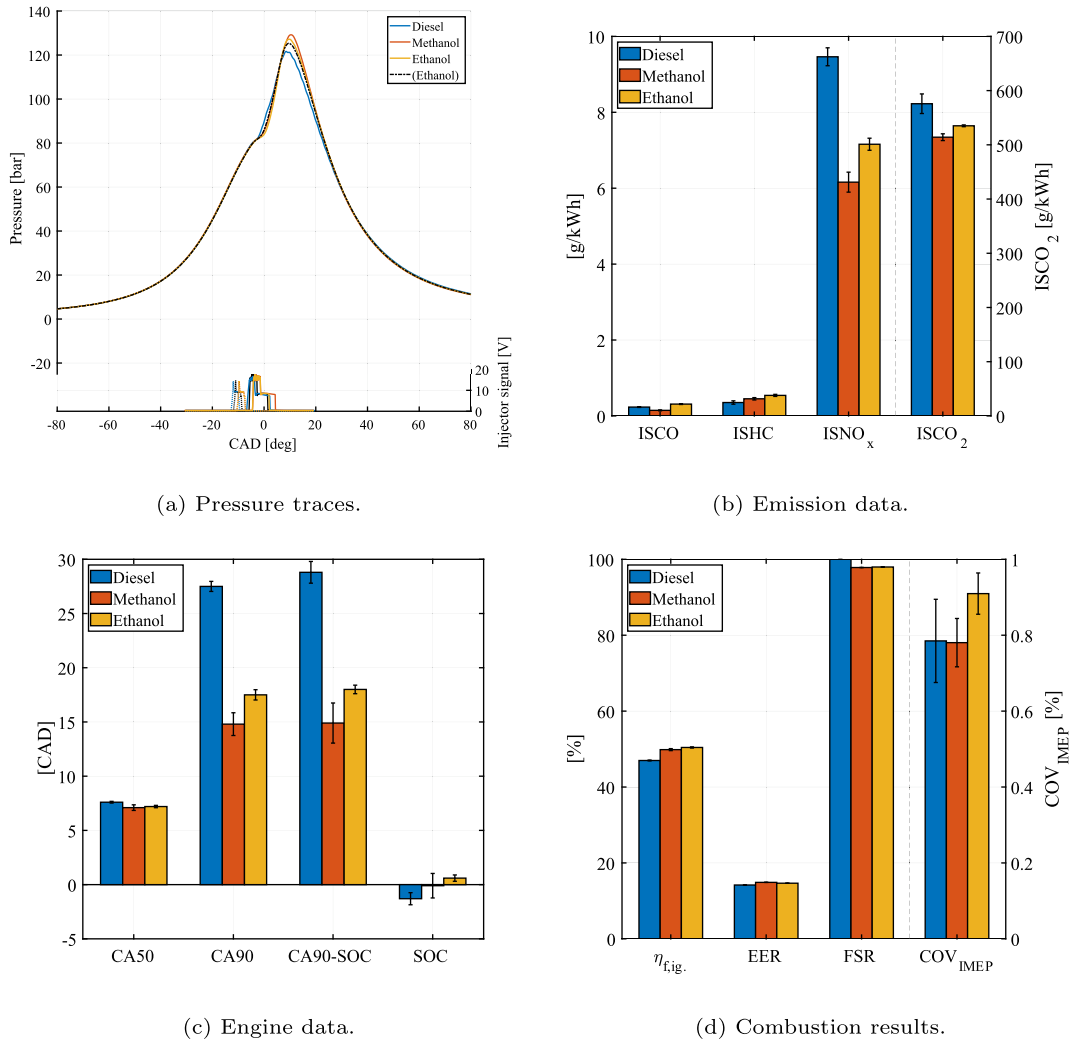

(a) Pressure traces.

(b) Emission data.

(c) Engine data.

(d) Combustion results.

Fig. 4. Pressure traces, selected emissions, engine data, and combustion data for methanol, ethanol and standard Diesel fuel at 1262 rpm and 172 Nm without EGR.

ethanol curves are very similar, which indicates very similar end of combustion behavior. Additionally, the shorter tails of the alcohol fuels are indicative of more complete combustion in the earlier stages and a more favorable thermodynamic positioning of the combustion process. It is preferable for combustion to occur such that the aRoHR curve is more symmetric and peaks close to *TDC* because this increases fuel efficiency and reduces emissions of soot, CO, and unburned hydrocarbons [37]. At high pressures and temperatures, mixing-controlled combustion chemistry is fast but limited by the availability of oxygen. The late combustion phase has significantly lower temperatures, low oxygen availability, and poorer mixing because it occurs after *EOI*. Late cycle oxidation is therefore unfavorable for Diesel combustion, leading to lower rates of soot oxidation and higher soot emissions [38].

The differences in the heat release curves for the studied fuels correspond to differences in their combustion behavior, which in turn produce different environments for the formation of emissions. These differences can be understood and characterized by studying engine out emissions and selected combustion parameters; some of the most important are shown in subFigs. 4b–4d.

Two particularly important variables in the context of this work are the indicated thermal fuel efficiency and indicated specific NO_x emissions. As shown in Fig. 4d, the $\eta_{f,ig}$ for methanol (49.9 %) and ethanol (50.5 %) was significantly higher than that for Diesel (47 %). The alcohol fuels delivered greater fuel efficiency than Diesel because of their more favorable combustion patterns, the greater symmetry of their aRoHR curves, and their shorter tails. This is supported by the results from the EER which calculates to 14.2 for Diesel 14.9 and 14.7 for methanol and ethanol respectively. Ethanol achieved a slightly higher efficiency than methanol because of its greater *LHV*. Studies have identified several factors that contribute to the higher fuel efficiency of alcohols. One is the cooling due to the higher heat of vaporization of alcohol-based fuels, which reduces the mean combustion temperature compared to that for Diesel and therefore reduces heat losses [39]. Another contribution is due to the oxygen content of the alcohols, which reduces the duration of the combustion and therefore lowers soot emissions. Fig. 4b also shows that the $ISNO_x$ emissions for methanol (6.2 g/kWh) and ethanol (7.2 g/kWh) were significantly lower than those for Diesel (9.5 g/kWh), corresponding to reductions of 35 and 24 %, respectively. This can be explained by considering the main driving forces of thermal NOx formation. Standard Diesel combustion generates temperatures above 2000 K and is associated with long residence times and high oxygen levels, all of which favor NO_x formation in accordance with the extended Zeldovich mechanism [40]. An earlier investigation found that the adiabatic flame temperature during Diesel combustion was significantly higher than for methanol [27], which suggests that methanol produces lower post-flame temperatures, leading to lower levels of NO_x formation. Diesel combustion also generates higher residence times than that of alcohol-based fuels because the combustion duration for Diesel combustion is almost twice that for methanol, as shown in Fig. 4c. Ethanol has a slightly longer combustion duration,

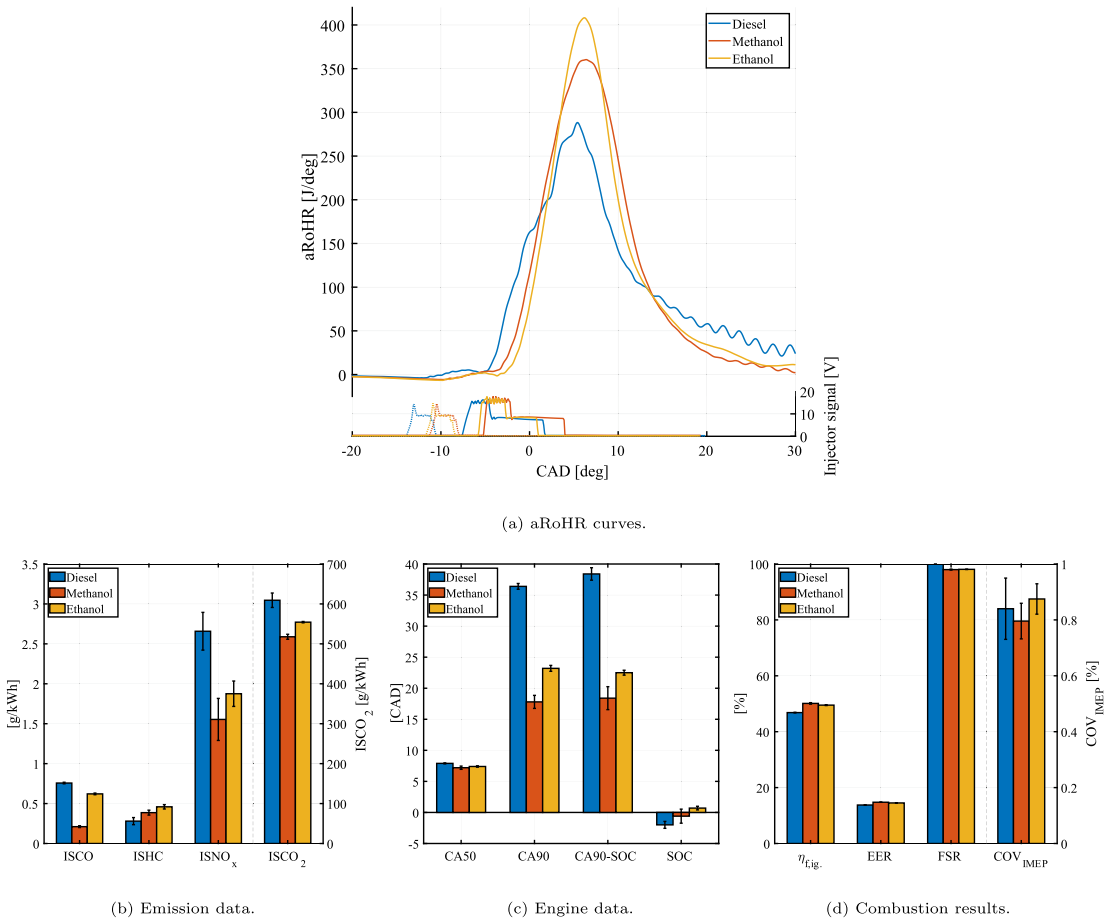

(a) aRoHR curves.

(b) Emission data.

(c) Engine data.

(d) Combustion results.

Fig. 5. aRoHR curves, emissions, engine data, and combustion data for methanol, ethanol, and standard Diesel fuel at 1262 rpm and 172 Nm with 20 % EGR.

resulting in slightly higher $ISNO_x$ emissions. Other emissions observed with the alcohol fuels, including indicated carbon monoxide and hydrocarbon emissions, were in the same range as those for Diesel. These emissions were considered less important in this stage of the investigation because modern exhaust gas after-treatment systems eliminate them very effectively. The combustion efficiency (η_{comb}) calculated for the alcohol fuels (99.8 %) was comparable to that for Diesel. However, the soot particulate emissions observed for the alcohols were much lower than those for Diesel (44-fold and 32-fold lower, respectively, for methanol and ethanol) and well below the requirements of the current Euro VI tailpipe emissions standards. The difference between methanol and Diesel can be explained by the shorter tail of the methanol aRoHR curve and the oxygen content of the alcohol fuels, both of which promote late cycle oxidation. Similar differences were observed at all speed-load points, so soot emissions are not considered further in this work. A more detailed analysis focusing on particulate sizes and size distributions will be needed to better understand the effects of using alcohol-based fuels in dual fuel systems on particulate emissions. A good measure of the alternative fuel's contribution to the engine's total work output in a dual fuel system is the fuel substitution ratio (*FSR*), which in

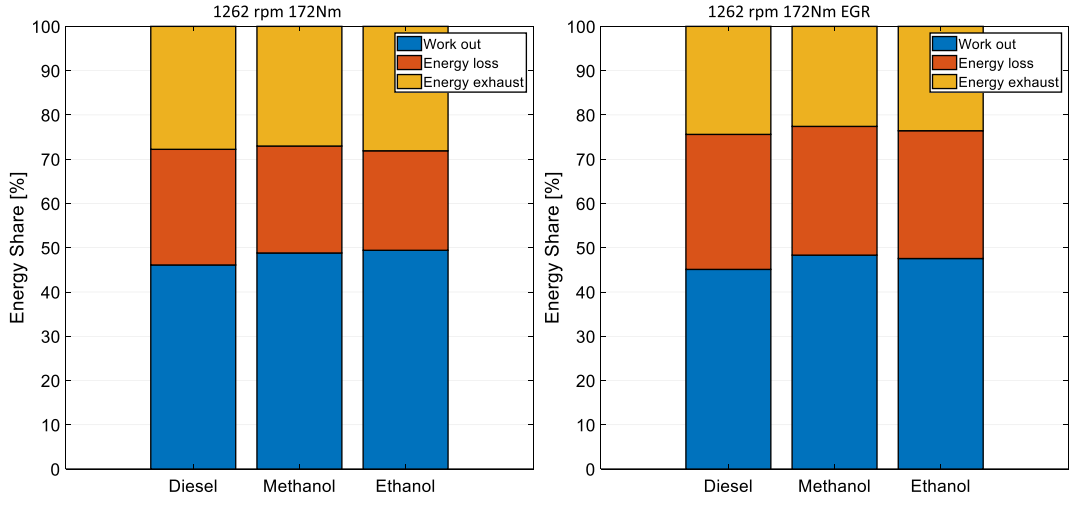

Fig. 6. Energy balances of methanol, ethanol and standard Diesel fuel at 1262 rpm 172 Nm with and without EGR.

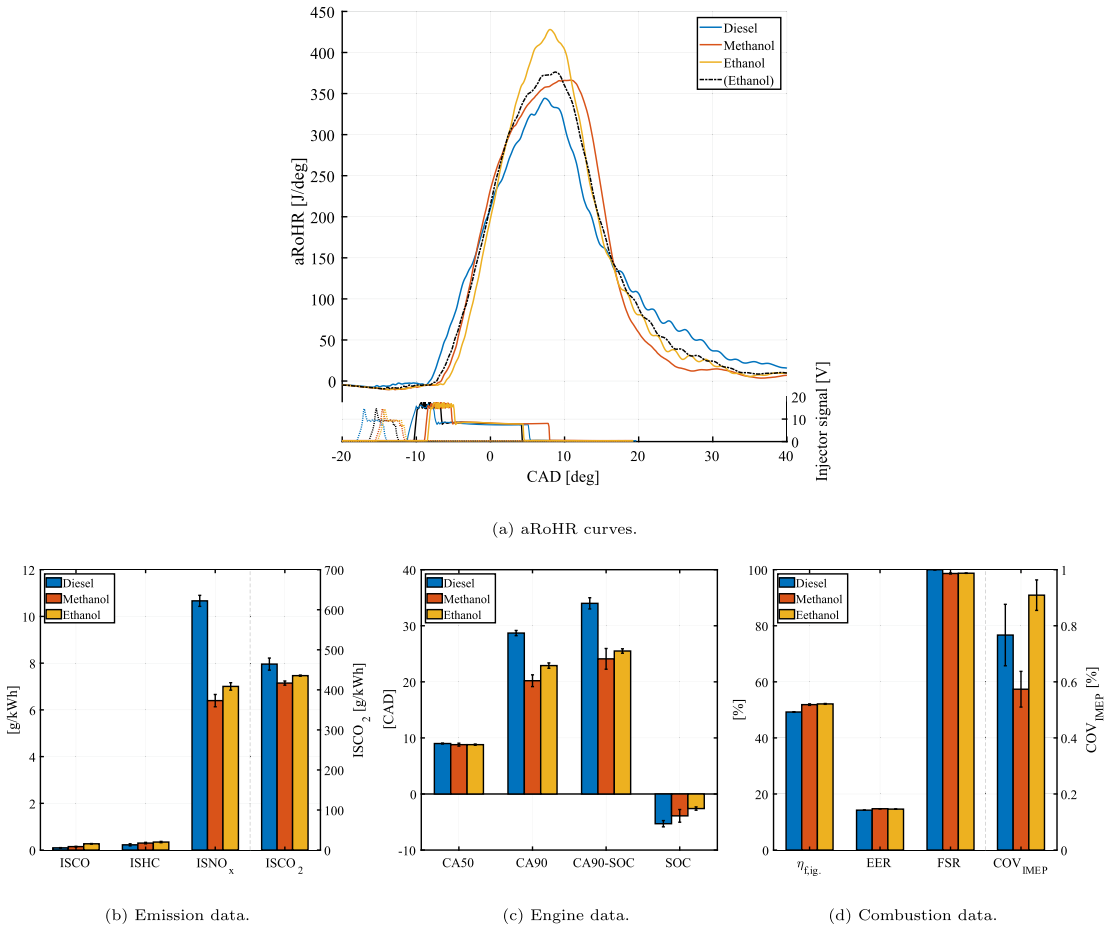

(a) aRoHR curves.

(b) Emission data.

(c) Engine data.

(d) Combustion data.

Fig. 7. aRoHR curves, emissions, engine data, and combustion data for methanol, ethanol, and Diesel at 1508 rpm and 285 Nm.

this case was almost 98 %. This shows that Diesel was only used to facilitate ignition; the vast majority of the combusted fuel was methanol or ethanol. All results obtained under these conditions can be found in Table 6 in the appendix.

Fig. 5 shows the aRoHR curves for the same fuels with 20 % EGR and an additional backpressure of 200 mbar to drive the EGR. This slightly increased the peak heat release rate for ethanol, slightly reduced that for Diesel, and had little effect on that for methanol. These small changes indicate that the amount of EGR used in this comparison had only a minor influence on the combustion process. The main purpose of using EGR is to reduce the oxygen concentration and temperature in the combustion chamber to avoid thermal NO_x formation. This also reduces the availability of oxygen for the combustion process, leading to the reduction in the heat release rate for Diesel. Table 7 in the appendix summarizes the results obtained under these conditions.

The engine out emissions and combustion parameters measured at the intermediate speed-load point with EGR are shown in sub-Figs. 5d. Using EGR at this speed-load point significantly reduced thermal NO_x formation, and Fig. 4b shows that both alcohol fuels performed better than Diesel under EGR conditions. EGR reduced the ISNOx emissions for Diesel to about 2.7 g/kWh while those for methanol and ethanol fell to 1.6 and 1.9 g/kWh, respectively. Further significant reductions in engine out NO_x emissions could be achieved by increasing the EGR rate. A moderate EGR rate was used in this case, however, to avoid major changes in the fuel efficiency, $\eta_{f.ig}$. Accordingly, $\eta_{f.ig}$ was unchanged from the case without EGR for Diesel and methanol, but that for ethanol was reduced by 1 percentage point.

Fig. 6 shows the energy balances for all fuels at 1262 rpm and 172 Nm with and without EGR. Without EGR the share of heat losses shown by energy loss in the figure, assuming that losses such as mechanical or friction were constant, was smaller for ethanol 22.5 % than for methanol 24.2 %. Even though the energy leaving the system through exhaust gases were slightly higher for ethanol, the efficiency was greater. When using the EGR system the share of heat losses was similar for ethanol at 28.9 % and methanol 29.1 % resulting in a lower $\eta_{f.ig}$ for ethanol under EGR conditions. Nevertheless, both alcohol fuels significantly outperformed Diesel in terms of $\eta_{f.ig}$ and ISNOx emissions, as shown in Fig. 5d. Using a much higher EGR rate would have reduced fuel efficiency and would also be likely to increase emissions of HC and CO. The use of EGR had little effect on most of the other studied variables, but the combustion duration increased in all cases. This shows that EGR slowed down combustion while reducing NO_x emissions. However, the combustion efficiency, COV, and FSR were largely unchanged.

3.1.2. aRoHR 1508 rpm 285 nm

A second round of experiments was performed at the high speed-load point (1508 rpm and 285 Nm), yielding the results shown in Fig. 7. The combustion phasing in this case was set to around 9 °aTDC, which is a bit later than that used in the intermediate load case; preliminary experiments indicated that this CA50 position slightly increased the engine's efficiency at high load.

The differences between the alcohols and Diesel were broadly similar to those seen in the intermediate load case, so the discussion below focuses on differences that can be attributed to the differing properties of the three studied fuels. Again, the two alcohol fuels clearly outperformed Diesel with respect to fuel efficiency and NO_x emissions, and also yielded very low soot emissions. However, the aRoHR curves for the high load case differed in some important respects from those for the intermediate load case, and are therefore described in detail.

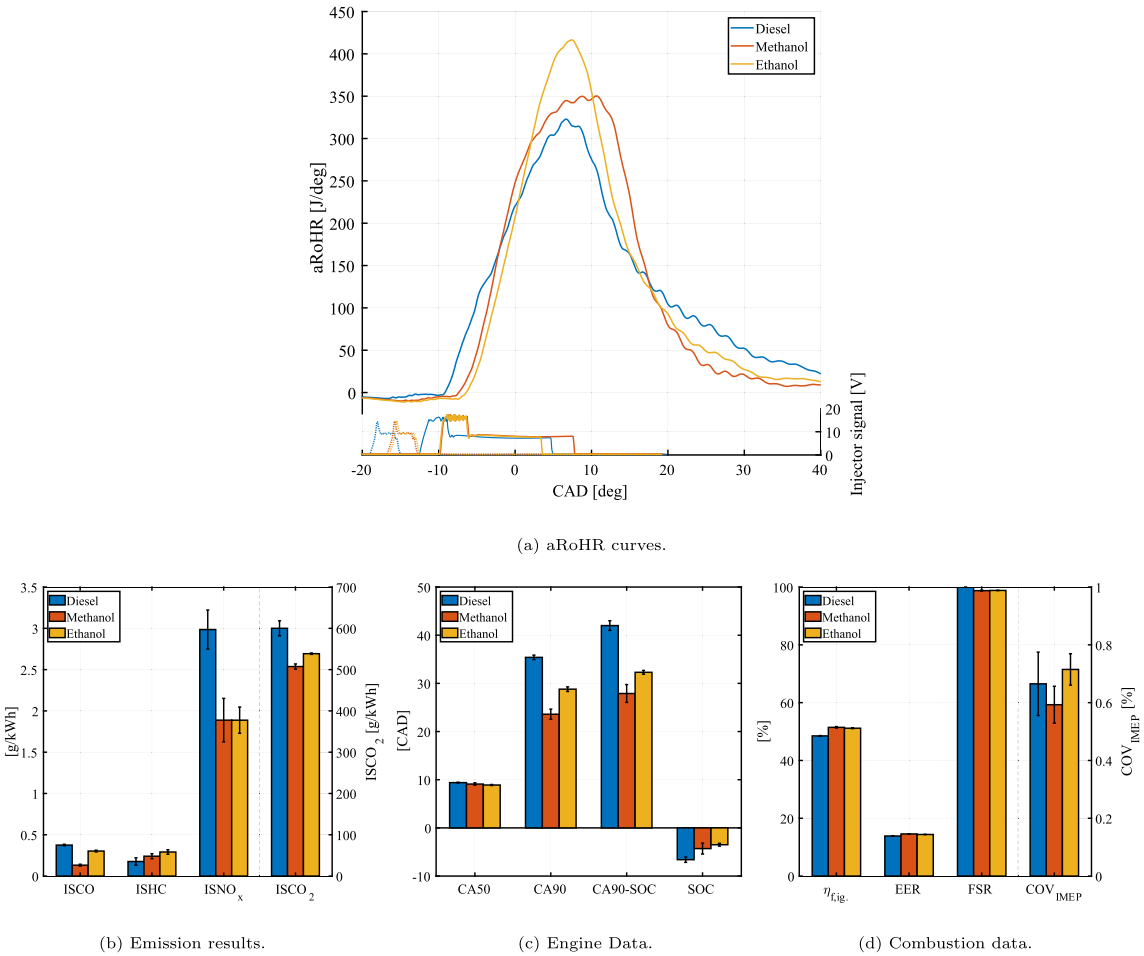

(a) aRoHR curves.

(b) Emission results.

(c) Engine Data.

(d) Combustion data.

Fig. 8. aRoHR curves, emissions, engine data, and combustion data for methanol, ethanol, and Diesel at 1508 rpm and 285 Nm with 20 % EGR.

Sub-Fig. 7a presents the *aRoHR* curves for the high load case. The higher load made it necessary to inject more fuel into the cylinder but the injection pressure was held constant at 1250 bar; consequently, the time scale differs from that for the intermediate load case. Following the small increase in heat release from the Diesel pilot, the main fuel injection causes a small decrease in heat release because of the initial evaporation of the fuel. During the free-flame phase, when the combusting fuel jets propagate towards the piston bowl, the slope of the curve reflects the speed of the combustion. The *aRoHR* curve for Diesel has a typical shape until the jets hit the piston bowl at around 3 °baTDC. Afterwards, the combustion speed is slightly reduced. The curve for ethanol does not exhibit such a clear transition, but the rate of heat release declines after 5 °aTDC, indicating the disappearance of the free-flame jet. The transition is more visible in the methanol curve; it occurs at around 4 °aTDC, and the maximum rate of heat release (around 370 J/deg) occurs at about 12 °aTDC. The peak heat release for ethanol occurs slightly earlier (around 8 °aTDC) and is somewhat higher (425 J/deg) than that for methanol. The higher peak for ethanol is again due to its greater *LHV*, which increases the rate of energy injection per CAD; the faster combustion of ethanol can be attributed to the different chemical structures of methanol and ethanol. As in the intermediate load case, additional experiments were conducted in which the ethanol injection pressure was reduced to equalize its rate of energy injection with that for methanol (see the dash-dotted aRoHR curve). This made the ethanol combustion pattern more similar to that for methanol, as was also observed at the intermediate speed-load point. The main differences between the tested fuels are seen in the tail of the combustion process: again, methanol yielded a shorter tail and a shorter overall combustion duration. All three plotted curve tails are shorter than that for Diesel.

Interestingly, the unusual sharp increase in the rate of heat release curve following the flame-wall interaction event seen for Diesel in the intermediate load case is clearly visible for both Diesel and ethanol in the high load case. This supports the hypothesis that this effect is caused by the experimental set-up rather than any property of the fuel.

As noted previously the differences in the fuels' heat release curves can be linked to different environments in the combustion chamber and thus differences in emissions. The engine out emissions and combustion parameters observed with the three fuels are shown in subFigs. 7b–7d. The trends are identical to those seen in the medium load case, but some details merit further discussion.

Fig. 7b shows that the NO_x emissions for the alcohol fuels (5.3 and 5.2 g/kWh for methanol and ethanol, respectively) were significantly lower than those for Diesel (about 9.3 g/kWh), corresponding to a reduction of about 43 %. Interestingly, the two alcohols yielded identical ISNOx values, unlike in the intermediate load case. The fuel efficiency, $\eta_{f,ig}$, achieved with the alcohols (51.6 % and 51.9 % for methanol and ethanol, respectively) was also significantly higher than that for Diesel (48.8 %), which is also reflected by the calculated EER values. The indicated carbon monoxide and hydrocarbon emissions for the alcohol fuels were in the same range as those for Diesel. However, the soot particulate emissions for the alcohol fuels were as low as those seen in the intermediate load case and significantly lower than those for Diesel, as shown in Table 8 (presented in the appendix). Additionally, Fig. 7c shows that the combustion duration (CA90-SOC) was significantly shorter for the alcohol fuels, but the reduction relative to Diesel was less pronounced than at the intermediate speed-load point: at 1262 rpm, the difference was around 1.9 ms but at 1508 it was only about 1.1 ms. This indicates that the overall combustion duration is more similar for higher load cases than for the

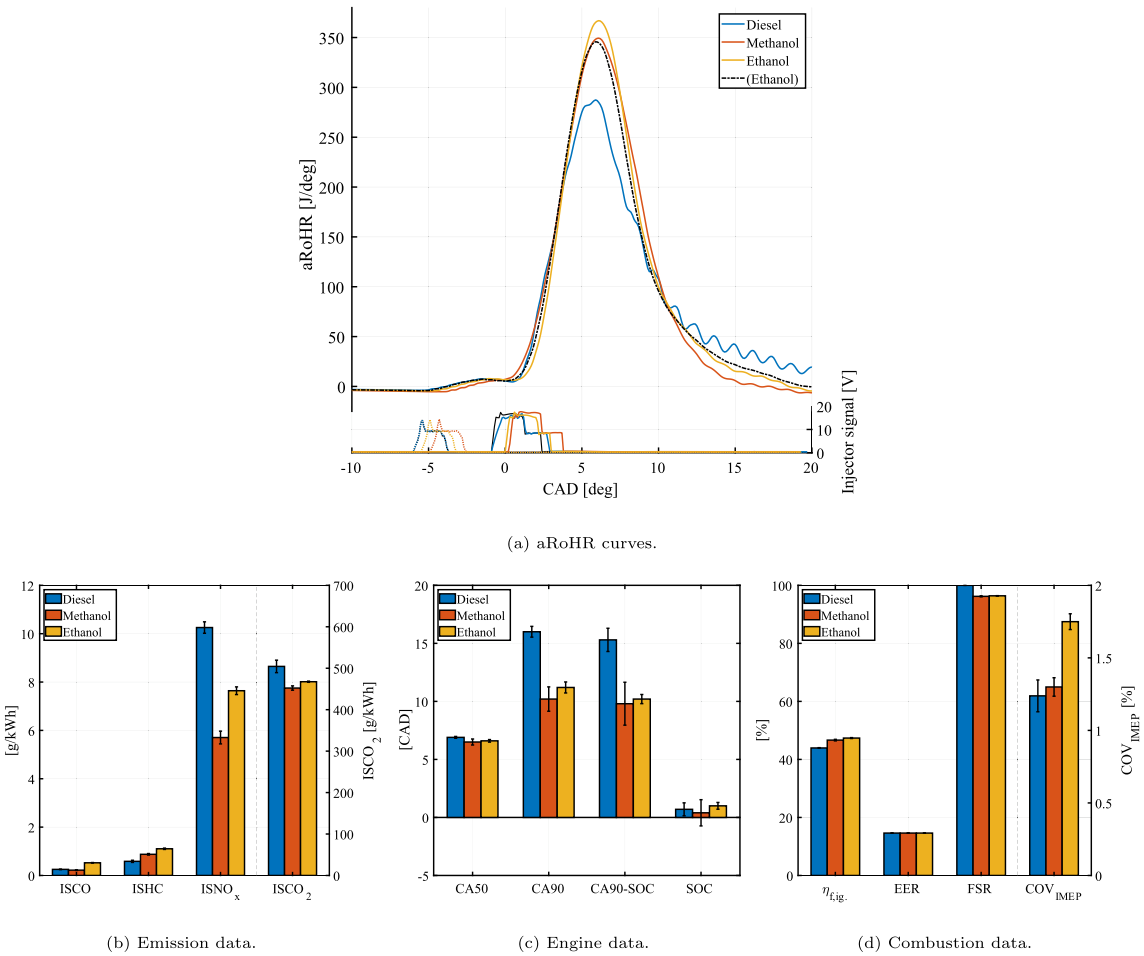

(a) aRoHR curves.

(b) Emission data.

(c) Engine data.

(d) Combustion data.

Fig. 9. aRoHR curves, emissions, engine data, and combustion data for methanol, ethanol, and Diesel at 871 rpm and 86 Nm.

medium load case. Again, the *FSR* were very high (over 98.7 %), slightly exceeding the value observed in the medium load case.

Fig. 8a shows the aRoHR curves obtained at the high speed-load point (1508 rpm and 285 Nm) with 20 % EGR and increased back pressure to drive the EGR. The curve shapes indicate that the combustion processes for each fuel were similar to those in the case without EGR, albeit with a lower peak heat release and a longer combustion duration for all fuels. The combustion phasing was kept constant at about 9 °aTDC. Key settings and results for the case with EGR are presented in Table 9 in the appendix.

Using EGR at this speed-load point significantly reduced NO_x formation. Fig. 4b shows that both alcohol fuels performed better than Diesel under EGR conditions. The $ISNO_x$ emission for Diesel fell to about 2.98 g/kWh while that for methanol and ethanol fell to 1.88 and 1.89 g/kWh, respectively. The significant difference between the alcohol fuels and Diesel persisted under EGR conditions: the $ISNO_x$ emissions with methanol and ethanol were around 27 % lower than those for Diesel. The fuel efficiency ($\eta_{f,ig}$) for Diesel and methanol was almost unchanged by the use of EGR, but that for ethanol fell by around 1 percentage point, all of which is once again by the results obtained for the EER. Despite this, both alcohol fuels significantly outperformed Diesel, as shown in Fig. 8d. The combustion duration increased in all cases, indicating that EGR slowed down combustion while reducing NO_x emissions. Combustion efficiency, COV, and FSR were largely unchanged, however.

3.1.3. aRoHR 871 rpm 87 Nm

To comprehensively assess the dual-fuel concept, experiments were also performed at a low speed-load point (871 rpm and 86 Nm of torque). Fig. 9a presents the results obtained under these conditions. The general results are consistent with the findings discussed previously, but some outcomes specific to these low load conditions warrant further analysis. The combustion phasing was kept constant at 7 °aTDC because previous studies indicated that this phasing results in good efficiency. Table 10 in the appendix summarizes the results obtained at the low load operating point.

Sub-Fig. 9a presents the heat release curves obtained at the low speed-load operating point without EGR. Experiments were conducted using an injection pressure of 1250 bar for all fuels, and separately, with an injection pressure of 1000 bar to compensate for the greater LHV. The alcohol heat release curves are very symmetrical, but their timings differ slightly. As noted previously, it is preferable for the aRoHR curve to be symmetric and to peak as close TDC as possible. Under low load conditions, methanol has both the latest injection timing and the earliest SOC, and thus has the lowest ignition delay of the three tested fuels; the ignition delay for ethanol is significantly longer. The peak heat release rate of methanol and ethanol is significantly greater than that for Diesel, which can be related to the properties of the fuels, the fuel–air mixing, and the injector geometries. Ethanol exhibited the highest heat release rate (around 370 J/deg) because its LHV is higher than that of methanol (for which the peak heat release rate was just under 350 J/deg). The peak heat release rate for Diesel was significantly lower (around 280 J/deg). When the rate of energy injection for ethanol was adjusted to equal that of methanol, the form of the left-hand part of the aRoHR curve (which includes the ignition and free flame phases, and potentially the flame wall interaction) was such that it was difficult to say whether a flame-wall interaction had occurred because the injection duration was very short (around 0.7 ms or less). Generally are the HR curves much more similar at low load due to the very short fuel injection event.

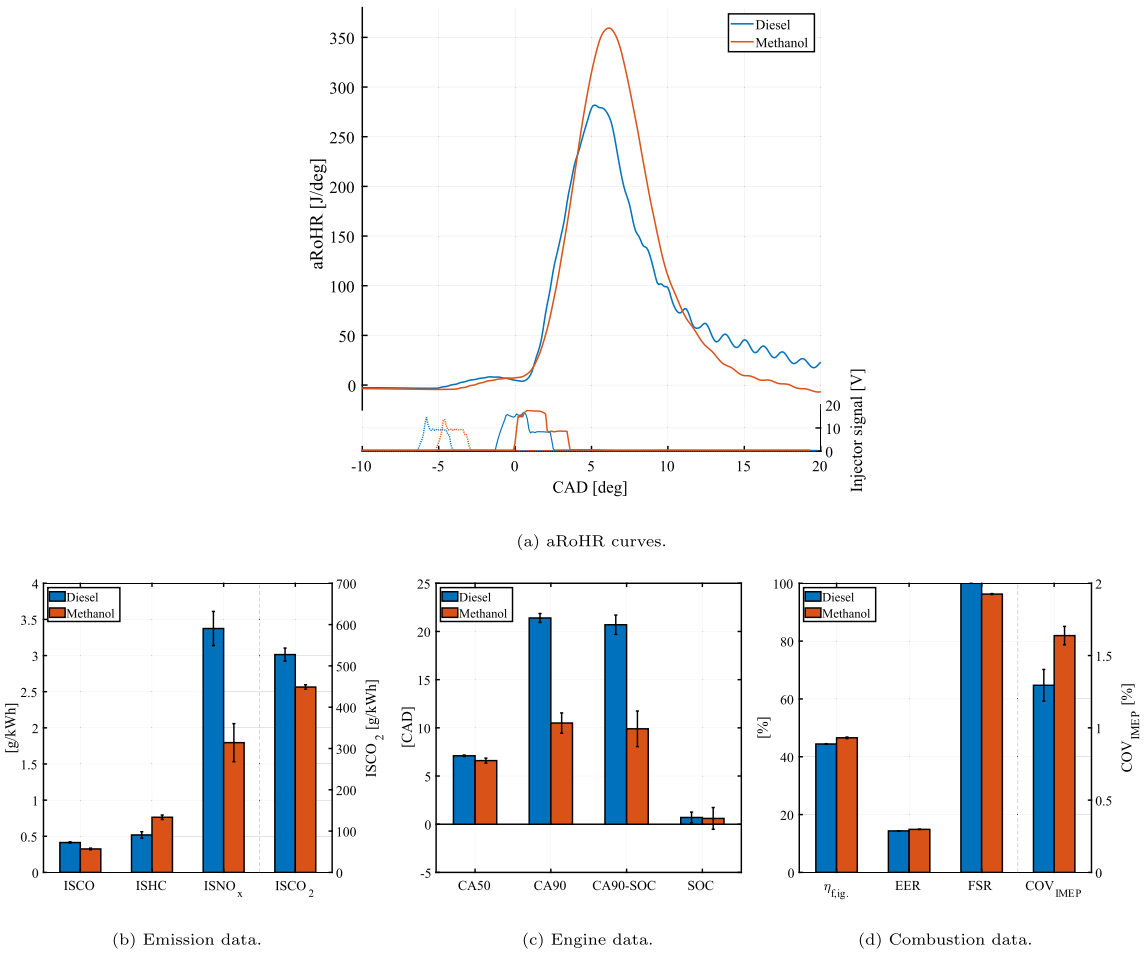

(a) aRoHR curves.

(b) Emission data.

(c) Engine data.

(d) Combustion data.

Fig. 10. aRoHR curves, emissions, engine data, and combustion data for methanol, ethanol, and Diesel at 871 rpm and 86 Nm with 20 % EGR.

As noted when discussing the intermediate and high speed-load points, differences in heat release profiles correspond to difference in combustion and thus differences in the conditions under which emissions are formed. Selected engine out emissions and combustion parameters are presented in subFigs. 9b–c. The results obtained are consistent with those for the intermediate and high speed-load cases, and therefore are not discussed at length; more detailed results are presented in Table 10 in the appendix. It should be noted that the alcohol fuels outperformed Diesel as before; $ISNO_x$ emissions for methanol and ethanol were around 40 % and 25 % lower, respectively, than for Diesel, while the indicated thermal fuel efficiency for the alcohols was significantly higher. Diesel achieved an efficiency of just under 44 %, whereas ethanol and methanol achieved efficiencies of 47.4 % and 46.6 %, respectively, in line with the calculated EER results. Interestingly, the percentage point differences in efficiency between the three fuels were fairly consistent across all three studied speed-load cases, with ethanol outperforming both Diesel and methanol. The combustion durations for the alcohols were significantly lower than for Diesel. The outcomes with respect to soot emissions were similar to those in the other two speed-load cases; again, both alcohols yielded soot emissions well below the upper limit mandated by current regulations. The calculated η_{comb} was 99.8 % for both Diesel and the alcohol fuels. This was expected because of the similar HC and CO emissions for the three fuels. The FSR for the alcohols was almost 96 %, which is lower than in the other two load cases because the mass of Diesel fuel injected during the pilot was kept constant but the mass of alcohol injected varied with the load. Nevertheless, this is a promising results, especially given that the engine exhibited acceptable combustion stability under low load; the COV values were slightly higher than in the other two load cases but remained below 2 %. The slight increase in cycle to cycle variation may be due to the small quantities of fuel injected at low load. Slightly increasing the mass of Diesel fuel injected during the pilot can have a stabilizing effect under such conditions.

Fig. 10a presents the results obtained at the low speed-load point (871 rpm and 86 Nm) with 20 % EGR. No usable data for ethanol could be obtained under these conditions because the air charge temperature decreased significantly due to the use of EGR and the Diesel pilot injection produced insufficient heat to consistently induce stable combustion of the main ethanol injection. Increasing the mass of Diesel fuel injected in the pilot would have improved combustion stability but made it difficult to meaningfully compare the results obtained to those for other fuels and speed-load points. This was the only case in which there were clear problems with the ignition of one of the alcohol fuels. The combustion phasing was kept constant at 7 °aTDC. Table 11 in the appendix summarizes the results obtained in this case.

Using EGR at this speed-load point significantly reduced thermal NO_x formation. Fig. 9b shows that methanol performed better than Diesel under EGR conditions, as also occurred in the intermediate and high speed-load cases. EGR reduced the $ISNO_x$ emissions for both Diesel and methanol by around 47 %, to around 3.40 g/kWh and 1.80 g/kWh, respectively. However, it had very little effect on $\eta_{f,ig}$ for either fuel. Most of the other studied variables were unchanged in relative terms when comparing methanol and ethanol to Diesel, but the combustion duration increased for Diesel while remaining almost unchanged for methanol. EGR thus slowed down the combustion of Diesel but had little effect on methanol combustion. The combustion efficiency and FSR were similar to those in the case without EGR, but the COV for methanol increased slightly, indicating a reduction in combustion stability.

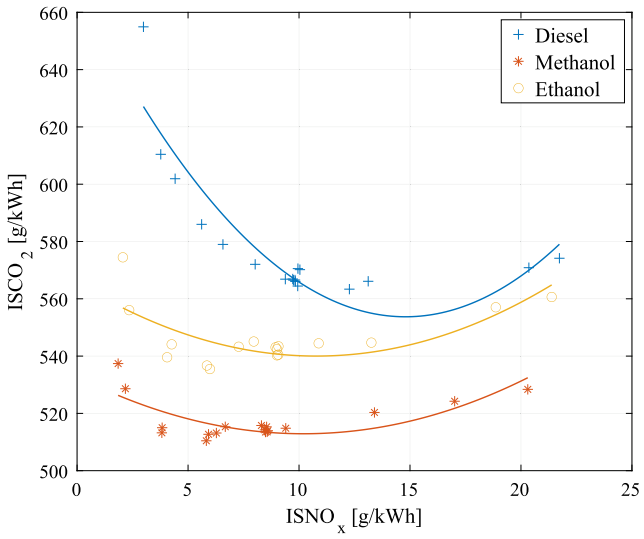

Fig. 11. $ISCO_2$ and ISNOx emissions for reference Diesel combustion and dual fuel combustion of methanol and ethanol.

3.2. Summary of the results

Fig. 11 summarizes the results of an investigation varying injection pressure, injection duration and injection timing over a wider range, using the studied dual fuel combustion system with methanol and ethanol as well as conventional Diesel combustion at the intermediate speed-load. The figure shows how the tailpipe $ISCO_2$ and $ISNO_x$ emissions varied as the injection pressure and timing changed; second order polynomials were used to fit curves for each fuel. The two alcohols clearly produce lower emissions than Diesel in all cases. For example, the densest cluster of Diesel datapoints is in the vicinity of 10 g/kWh $ISNO_x$ and 570 g/kWh $ISCO_2$.

Conversely, the densest cluster of methanol datapoints is approximately centered on 8 g/kWh $ISNO_x$ and 510 g/kWh $ISCO_2$. Thus, for a given speed-load operating point, the dual fuel engine produces roughly 20% lower NO_x emissions than conventional Diesel combustion while simultaneously reducing CO_2 emissions by about 10 %. This reduction stems from a higher $\eta_{f,ig}$ for methanol and ethanol, which was due to the greater latent heat of vaporization and a faster combustion reflected by the greater EER, but also due to the lower amount of carbon in the fuel. To comply with future legislation and reduce the need for large exhaust gas aftertreatment systems, it may be necessary to limit NO_x emissions to 5 g/kWh; under such conditions, the use of alcohols reduced CO_2 emissions by 14 % relative to Diesel combustion. Additionally, the soot emissions for alcohol combustion were much lower (usually by a factor of 40 or more) than those for Diesel combustion. *HC* and *CO* emissions for the alcohols were slightly higher than for Diesel, and would have to be taken care of by the aftertreatment system as well. Nowadays these systems require a minimal exhaust gas temperature of around 250 °C to operate efficiently [41]. The exhaust gas temperatures for the alcohol fuels are generally lower than for Diesel but never fell below this limit in any of the experiments.

4. Conclusions

A direct comparison with other technologies is difficult at this stage, but some general advantages of this technology towards HDPI or RCCI are the responsiveness and the generally low HC and CO emissions at simultaneously high FSRs. The following conclusions can be drawn from the results presented here:

- The presented dual-fuel concept with two separate direct injectors and a separate common rail systems works very well over a wide range of speed-load conditions
- Methanol and ethanol outperform Diesel in terms of efficiency, nitrogen oxide emissions, and PM emissions under the same operating conditions. This can mainly be attributed to the differences in the fuels' heat of vaporization and oxygen content and the increased turbulence created from the higher mass flow rate during the injection event, which cause the alcohols to have much higher rates of combustion at lower combustion temperatures.
- Hydrocarbon and CO emissions are slightly elevated when using ethanol or methanol but remain in the same range as for Diesel combustion.
- Very high fuel substitution ratios exceeding 95 % were achieved, indicating that GHG emissions could be reduced substantially by using renewable alcohol fuels
- The pilot Diesel injection could be replaced with HVO to reduce fossil fuel dependency
- Tailpipe CO_2 emissions were significantly lower at similar NO_x emission levels

Table 4
Specifications of Injectors used.

Injector	Name	Details
Bosch (side)	CRI2-18	3-hole, asymetric
Delphi (alcohols)	F3 (DFI5)	8-hole, 4.65 l/min at 100 bar, 147°
Delphi (Diesel)	F2 (DFI21)	6-hole, 2.3 l/min at 100 bar, 150°

CRediT authorship contribution statement

Michael Saccullo: Investigation, Writing - original draft, Writing - review & editing, Formal analysis, Visualization, Methodology. **Andreas Nygren:** Writing - review & editing, Formal analysis, Visualization. **Timothy Benham:** Investigation, Writing - review & editing. **Ingemar Denbratt:** Supervision, Funding acquisition, Writing - review & editing, Resources.

Declaration of Competing Interest

The authors declare that they have no known competing financial interests or personal relationships that could have appeared to influence the work reported in this paper.

Acknowledgement

Financial support from Swedish Energy Agency and is gratefully acknowledged. The cooperation with AB Volvo, Loge AB, Delphi and Bosch is also gratefully acknowledged as partners in the project. Further grateful acknowledgement goes to the assistance from the research engineers at Chalmers and all project partners involved. The simulations were performed on resources at Chalmers Centre for Computational Science and Engineering (C3SE) provided by the Swedish National Infrastructure for Computing (SNIC).

Appendix A

Table 5
Accuracy of the AVL AMA i60 R1C-EGR emissions measurement system.

Instrument	Emission	min [ppm,%]	max [ppm,%]
CLD i60 HHD SLQ	NO	0 – 10	10000
CLD i60 HHD SLQ	NO_x	0 – 10	10000
Cutter FID i60 HHD	CH_4	10	20000
Cutter FID i60 HHD	THC	10	20000
IRD i60 CO_2 H	CO_2	0 – 0.5%	20%
IRD i60 CO_2 L	CO_2	0 – 0.1%	6%
IRD i60 CO L	CO	0 – 50	5000
PMD i60 O_2	O_2	0 – 1%	25%

Table 6
Operating conditions for Diesel, methanol and ethanol, at 1250 bar and 1000 bar (ethanol) injection pressure, at 1262 rpm and 172 Nm without EGR.

Settings		**Diesel**	**Methanol**	**Ethanol**	**(Ethanol)**
Speed	[rpm]	1262	1262	1262	1262
Torque	[Nm]	172.3	172.0	171.8	172.4
Intake temperature, T_{in}	[°C]	29.5	29.8	29.3	29.4
Main Fuel		Diesel	Methanol	Ethanol	Ethanol
Injector	type	Delphi F2	Delphi F3	Delphi F3	Delphi F3
Injection pressure, P_{main}	[bar]	1250	1250	1250	1000
SOI_m	[°bTDC]	6.0	3.6	3.7	5.1
Injection duration	[ms]	1.189	1.172	0.857	0.957
Fuel mass flow, $\dot{m}_m$	$[\frac{mg}{stroke}]$	117.03	247.41	195.78	195.6
Energy injected per CAD	$[\frac{J}{CAD}]$	561	500	722	645
Igniter Fuel		Diesel	Diesel	Diesel	Diesel
SOI_i	[°bTDC]	12.0	9.6	9.8	11.1
Fuel mass flow, $\dot{m}_i$	$[\frac{mg}{stroke}]$	2.17	2.41	2.27	2.24
Measurement Results					
$\eta_{f.ig}$	[%]	47.00	49.85	50.46	50.43
η_{comb}	[%]	99.8	99.9	99.8	99.8
$ISNO_x$	[g/kWh]	9.46	6.16	7.16	6.56
$ISCO_2$	[g/kWh]	575.8	514.1	535.1	536.0
ISHC	[g/kWh]	0.35	0.45	0.54	0.59
ISCO	[g/kWh]	0.23	0.15	0.31	0.31
ISSoot	[g/kWh]	0.0031	$7.06 * 10^{-5}$	$9.70 * 10^{-5}$	$9.18 * 10^{-5}$
CA50	[°aTDC]	7.6	7.1	7.2	7.2
CA90 - SOC	[CAD]	28.8	14.9	16.9	19.7
Fuel Substitution Ratio (FSR)	[%]	0	97.8	98.0	98.0
Peak pressure, P_{peak}	[bar]	123.4	129.5	127.6	125.6
EER		14.18	14.88	14.72	14.66
COV	[%]	0.79	0.78	0.91	0.97
$T_{exhaust}$	[°C]	360	329	341	342

Table 7
Operating conditions for Diesel, methanol and ethanol at 1262 rpm and 172 Nm with 20 % EGR.

Settings		**Diesel**	**Methanol**	**Ethanol**
Speed	[rpm]	1262	1262	1262
Torque	[Nm]	171.9	171.9	172.0
Intake temperature, T_{in}	[°C]	29.5	33.5	32.0
Main Fuel		Diesel	Methanol	Ethanol
Injector	type	Delphi F2	Delphi F3	Delphi F3
Injection pressure, P_{main}	[bar]	1250	1250	1250
SOI_m	[°bTDC]	7.0	4.5	4.9
Injection duration	[ms]	1.221	1.212	0.884
Fuel mass flow, $\dot{m}_m$	$[\frac{mg}{stroke}]$	119.96	253.53	200.67
Energy injected per CAD	$[\frac{J}{CAD}]$	560	496	717
Igniter Fuel		Diesel	Diesel	Diesel
SOI_i	[°bTDC]	13.0	10.5	11.0
Fuel mass flow, $\dot{m}_i$	$[\frac{mg}{stroke}]$	2.09	2.27	2.17
Measurement Results				
$\eta_{f.ig}$	[%]	46.83	50.12	49.51
η_{comb}	[%]	99.8	99.9	99.8
$ISNO_x$	[g/kWh]	2.66	1.55	1.88
$ISCO_2$	[g/kWh]	609.2	517.8	554.4
ISHC	[g/kWh]	0.28	0.39	0.46
ISCO	[g/kWh]	0.76	0.21	0.62
ISSoot	[g/kWh]	0.044	$1.20 * 10^{-4}$	–
CA50	[°aTDC]	7.9	7.2	7.4
CA90 - SOC	[CAD]	38.4	18.4	22.5

(*continued on next page*)

Table 7 (*continued*)

Settings		Diesel	Methanol	Ethanol
Fuel Substitution Ratio (FSR)	[%]	0	98.00	98.09
Peak pressure, P_{peak}	[bar]	122.2	128.3	125.9
EER		13.77	14.76	14.51
COV	[%]	0.84	0.80	0.88
$T_{exhaust}$	[°C]	391	356	368

Table 8
Operating conditions for Diesel, methanol and ethanol, at 1250 bar and 1000 bar (ethanol) injection pressure, at 1508 rpm and 285 Nm without EGR.

Settings		Diesel	Methanol	Ethanol	(Ethanol)
Speed	[rpm]	1508	1508	1508	1508
Torque	[Nm]	284.7	284.6	285.2	285.2
Intake temperature, T_{in}	[°C]	30.0	30.2	29.9	29.9
Main Fuel		Diesel	Methanol	Ethanol	Ethanol
Injector	type	Delphi F2	Delphi F3	Delphi F3	Delphi F3
Injection pressure, P_{main}	[bar]	1250	1250	1250	1000
SOI_m	[°bTDC]	10.7	8.1	7.9	9.6
Injection duration [ms]	1.836	1.875	1.448	1.624	
Fuel mass flow, $\dot{m}_m$	$[\frac{mg}{stroke}]$	183.53	389.90	311.04	310.97
Energy injected per CAD	$[\frac{J}{CAD}]$	477	492	679	605
Igniter Fuel		Diesel	Diesel	Diesel	Diesel
SOI_i	[°bTDC]	17.3	14.7	14.5	15.7
Fuel mass flow, $\dot{m}_i$	$[\frac{mg}{stroke}]$	2.08	2.35	2.19	2.17
Measurement Results					
$\eta_{f.ig}$	[%]	49.24	51.87	52.13	52.26
η_{comb}	[%]	99.9	99.9	99.9	99.9
$ISNO_x$	[g/kWh]	10.7	6.4	7.0	6.4
$ISCO_2$	[g/kWh]	557.2	500.3	522.6	520.4
$ISHC$	[g/kWh]	0.22	0.30	0.34	0.37
$ISCO$	[g/kWh]	0.10	0.15	0.27	0.25
$ISSoot$	[g/kWh]	$7.48 * 10^{-4}$	$1.95 * 10^{-5}$	$2.49 * 10^{-4}$	$4.13 * 10^{-4}$
CA50	[°aTDC]	9.0	8.8	8.8	8.9
CA90 - SOC	[CAD]	34.0	24.1	25.5	28.9
Fuel Substitution Ratio (FSR)	[%]	0	98.7	98.8	98.8
Peak pressure, P_{peak}	[bar]	194.4	195.5	198.9	196.4
EER		14.23	14.74	14.61	14.55
COV	[%]	0.77	0.57	0.75	0.65
$T_{exhaust}$	[°C]	388	362	370	372

Table 9
Operating conditions for Diesel, methanol and ethanol at 1508 rpm and 285 Nm with 20 % EGR.

Settings		Diesel	Methanol	Ethanol
Speed	[rpm]	1508	1508	1508
Torque	[Nm]	285.4	285.3	284.9
Intake temperature, T_{in}	[°C]	34.2	40.9	38.6
Main Fuel		Diesel	Methanol	Ethanol
Injector	type	Delphi F2	Delphi F3	Delphi F3
Injection pressure, P_{main}	[bar]	1250	1250	1250
SOI_m	[°bTDC]	11.8	9.1	9.0
Injection duration	[ms]	1.922	1.957	1.495
Fuel mass flow, $\dot{m}_m$	$[\frac{mg}{stroke}]$	191.58	406.72	320.99
Energy injected per CAD	$[\frac{J}{CAD}]$	476	493	679
Igniter Fuel		Diesel	Diesel	Diesel
SOI_i	[°bTDC]	18.4	15.8	15.6
Fuel mass flow, $\dot{m}_i$	$[\frac{mg}{stroke}]$	2.06	2.26	2.12

(*continued on next page*)

Table 9 (*continued*)

Settings		Diesel	Methanol	Ethanol
Measurement Results				
$\eta_{f.ig}$ [%]	48.49	51.45	51.16	
η_{comb}	[%]	99.9	99.9	99.9
$ISNO_x$	[g/kWh]	2.99	1.89	1.89
$ISCO_2$	[g/kWh]	600.1	507.4	538.6
ISHC	[g/kWh]	0.18	0.24	0.29
ISCO	[g/kWh]	0.38	0.12	0.30
ISSoot	[g/kWh]	0.0074	$2.06 * 10^{-4}$	–
CA50	[°aTDC]	9.4	9.1	8.9
CA90 - SOC	[CAD]	42.0	27.9	32.3
Fuel Substitution Ratio (FSR)	[%]	0	98.8	98.8
Peak pressure, P_{peak}	[bar]	194.2	194.7	198.3
EER		13.86	14.57	14.39
COV	[%]	0.67	0.59	0.72
$T_{exhaust}$	[°C]	434.7	407.3	410.7

Table 10
Operting conditions for Diesel, methanol and ethanol, at 1250 bar and 1000 bar (ethanol) injection pressure, at 871 rpm and 86 Nm without EGR.

Settings		Diesel	Methanol	Ethanol	(Ethanol)
Speed	[rpm]	871	871	871	871
Torque	[Nm]	86.0	85.8	85.8	86.5
Intake temperature, T_{in}	[°C]	28.6	29.9	29.5	29.4
Main Fuel		Diesel	Methanol	Ethanol	Ethanol
Injector	type	Delphi F2	Delphi F3	Delphi F3	Delphi F3
Injection pressure, P_{main}	[bar]	1250	1250	1250	1000
SOI_m	[°bTDC]	0.2	-1.2	-0.9	0.0
Injection duration	[ms]	0.709	0.674	0.571	0.622
Fuel mass flow, $\dot{m}_m$	$[\frac{mg}{stroke}]$	64.93	134.55	106.82	106.88
Energy injected per CAD	$[\frac{MJ}{CAD}]$	756	686	856	787
Igniter Fuel		Diesel	Diesel	Diesel	Diesel
SOI_i	[°bTDC]	5.3	3.9	4.2	5.1
Fuel mass flow, $\dot{m}_i$	$[\frac{mg}{stroke}]$	2.06	2.33	2.22	2.22
Measurement Results					
$\eta_{f.ig}$	[%]	43.94	46.66	47.36	47.16
η_{comb}	[%]	99.7	99.8	99.6	99.6
$ISNO_x$	[g/kWh]	10.3	5.7	7.6	7.5
$ISCO_2$	[g/kWh]	605.3	542.6	560.9	561.4
ISHC	[g/kWh]	0.58	0.88	1.10	1.16
ISCO	[g/kWh]	0.25	0.22	0.52	0.72
ISSoot	[g/kWh]	0.0067	$8.35 * 10^{-5}$	$1.00 * 10^{-4}$	$8.48 * 10^{-5}$
CA50	[°aTDC]	6.9	6.5	6.6	6.5
CA90 - SOC	[CAD]	15.3	9.8	10.2	10.7
Fuel Substitution Ratio (FSR)	[%]	0	96.2	96.4	96.4
Peak pressure, P_{peak}	[bar]	78.1	82.1	80.8	79.8
EER		14.61	14.91	14.85	14.87
COV	[%]	1.24	1.3	1.85	1.65
$T_{exhaust}$	[°C]	271	252	256	257

Table 11
Operating conditions for Diesel and methanol at 871 rpm and 86 Nm with 20 % EGR.

Settings		**Diesel**	**Methanol**
Speed	[rpm]	871	871
Torque	[Nm]	86.0	85.9
Intake temperature, T_{in}	[°C]	30.0	30.3
Main Fuel		Diesel	Methanol
Injector	type	Delphi F2	Delphi F3
Injection pressure, P_{main}	[bar]	1250	1250
SOI_m	[°bTDC]	0.5	-0.8
Injection duration	[ms]	0.712	0.684
Fuel mass flow, $\dot{m}_m$	$[\frac{mg}{stroke}]$	64.61	136.71
Energy injected per CAD	$[\frac{MJ}{CAD}]$	749	687
Igniter Fuel		Diesel	Diesel
SOI_i	[°bTDC]	5.6	4.3
Fuel mass flow, $\dot{m}_i$	$[\frac{mg}{stroke}]$	2.03	2.33
Measurement Results			
$\eta_{f.ig}$	[%]	44.42	46.55
η_{comb}	[%]	99.7	99.8
$ISNO_x$	[g/kWh]	3.4	1.8
$ISCO_2$	[g/kWh]	602.7	512.9
$ISHC$	[g/kWh]	0.52	0.76
$ISCO$	[g/kWh]	0.41	0.32
$ISSoot$	[g/kWh]	0.011	$5.92 * 10^{-5}$
CA50	[°aTDC]	7.1	6.6
CA90 - SOC	[CAD]	20.7	9.9
Fuel Substitution Ratio (FSR)	[%]	0	96.26
Peak pressure, P_{peak}	[bar]	76.1	96.1
EER		14.35	14.88
COV	[%]	1.30	1.62
$T_{exhaust}$	[°C]	283	264

References

[1] HEI. Diesel Exhaust A Critical Analysis of Emissions. Exposure, and Health Effects 1995:1–69.
[2] Risk R, Workers Y, Workers O, Diesel Exhaust: Critical Analysis of Emissions, Exposure, and Health Effects - part 5 02.
[3] IPCC O, Edenhofer R, Pichs-Madruga Y, Sokona, E. Farahani S, Kadner K (eds.), Climate Change 2014: Mitigation of Climate Change. Contribution of Working Group III to the Fifth Assessment Report of the Intergovernmental Panel on Climate Change, Cambridge University Press, Cambridge, United Kingdom and New York, NY, USA, 2014. arXiv:arXiv:1011.1669v3, doi:10.1017/CBO9781107415416.
[4] Sarjovaara T, Alantie J, Larmi M. Ethanol dual-fuel combustion concept on heavy duty engine. Energy 2013;63(x):76–85. https://doi.org/10.1016/j.energy.2013.10.053.
[5] Ecklund O, Bechtold RL, Timbario TJ, McCallum PW, State-of-the-art report on the use of alcohols in diesel engines, SAE Technical Papersdoi:10.4271/840118.
[6] Liotta FJ, Montalvo DM, The effect of oxygenated fuels on emissions from a modern heavy-duty diesel enginedoi:https://doi.org/10.4271/932734. doi: 10.4271/932734.
[7] Pickett LM, Siebers DL, Non-sooting, low flame temperature mixing controlled DI diesel combustion, SAE transactions (724). doi:10.4271/2004-01-1399.
[8] Noehre C, Andersson M, Johansson B, Hultqvist A, Characterization of Partially Premixed Combustion, SAE Technical Paper, 2006-01-3412 (724) (2006) 776–790. doi:10.4271/2006-01-3412.
[9] Gao T, Divekar P, Asad U, Han X, Reader GT, Wang M, Zheng M, Tjong J. An Enabling Study of Low Temperature Combustion With Ethanol in a Diesel Engine. J Energy Resour Technol 2013;135(4):1–8. https://doi.org/10.1115/1.4024027.
[10] Alriksson M, Rente T, Denbratt I, Low Soot, Low NOx in a Heavy Duty Diesel Engine Using High Levels of EGR, SAE International (724).
[11] Çelebi Y, Aydin H, An overview on the light alcohol fuels in diesel engines, Fuel 236 (September 2018) (2019) 890–911. doi:10.1016/j.fuel.2018.08.138.
[12] Hansen AC, Zhang Q, Lyne PW. Ethanol-diesel fuel blends - A review. Bioresource Technol 2005;96(3):277–85. https://doi.org/10.1016/j.biortech.2004.04.007.
[13] Atadashi IM, Aroua MK, Aziz AA. High quality biodiesel and its diesel engine application: A review. Renewable Sustainable Energy Rev 2010;14(7):1999–2008. https://doi.org/10.1016/j.rser.2010.03.020.
[14] Siebers DL, Edwards C, Autoignition of Methanol and Ethanol Sprays under Diesel Engine Conditions, SAE Technical Paper doi:10.4271/870588.
[15] Li G, Zhang C, Li Y. Effects of diesel injection parameters on the rapid combustion and emissions of an HD common-rail diesel engine fueled with diesel-methanol dual-fuel. Appl Thermal Eng 2016;108:1214–25. https://doi.org/10.1016/j.applthermaleng.2016.08.029.
[16] Vallinayagam R, Vedharaj S, Yang WM, Roberts WL, Dibble RW. Feasibility of using less viscous and lower cetane (LVLC) fuels in a diesel engine: A review. Renewable Sustainable Energy Rev 2015;51:1166–90. https://doi.org/10.1016/j.rser.2015.07.042.
[17] Jia Z, Denbratt I. Experimental investigation into the combustion characteristics of a methanol-Diesel heavy duty engine operated in RCCI mode. Fuel 2018;226 (March):745–53. https://doi.org/10.1016/j.fuel.2018.03.088.
[18] Reitz RD, Duraisamy G. Review of high efficiency and clean reactivity controlled compression ignition (RCCI) combustion in internal combustion engines. Progress Energy Combust Sci 2014;46:12–71. https://doi.org/10.1016/j.pecs.2014.05.003.
[19] McTaggart-Cowan G, Bushe WK, Hill PG, Munshi SR. NOx reduction from a heavy-duty diesel engine with direct injection of natural gas and cooled exhaust gas recirculation. Int J Eng Res 2004;5(2):175–91. https://doi.org/10.1243/146808704773564578.
[20] McTaggart-Cowan G, Mann K, Wu N, Munshi S, An efficient direct-injection of natural gas engine for heavy duty vehicles, SAE Technical Papers 1. doi:10.4271/2014-01-1332.
[21] Ullman TM, Terry L, Hare Charles T, Baines, Emissions from Direct-Injected Heavy-Duty Methanol-Fueled Engines (One Dual-Injection and One Spark-Ignited) and a Comparable Diesel Engine, SAE International doi:10.4271/820966.
[22] Lorusso JA, Cikanek HA, Direct Injection Ignition Assisted Alcohol Engine, SAE Technical Paperdoi:10.4271/880495.
[23] Giramondi N, Mihaescu M, Erlandsson AC, Jäger A, CFD-Driven Preliminary Investigation of Ethanol-Diesel Diffusive Combustion in Heavy-Duty Engines, SAE Technical Paper Series 1. doi:10.4271/2019-01-2192.
[24] Wissink M, Reitz RD. Direct Dual Fuel Stratification, a Path to Combine the Benefits of RCCI and PPC. SAE Int J Eng 2015;8(2). https://doi.org/10.4271/2015-01-0856. pp. 2015–01–0856.
[25] Wissink M, Reitz R. Exploring the Role of Reactivity Gradients in Direct Dual Fuel Stratification. SAE Int J Eng 2016;9(2). https://doi.org/10.4271/2016-01-0774. 2016–01–0774.
[26] J.B. Heywood, Internal Combustion Engine Fundementals, Vol. 21, 1988. doi: 10987654.

[27] Saccullo M, Benham T, Denbratt I, Dual Fuel Methanol and Diesel Direct Injection HD Single Cylinder Engine Tests, SAE Technical Papers 2018-April (2018) 1–12. doi:10.4271/2018-01-0259.
[28] Savitzky A, Golay MJ. Smoothing and Differentiation of Data by Simplified Least Squares Procedures. Anal Chem 1964;36(8):1627–39. https://doi.org/10.1021/ac60214a047.
[29] Ghojel J, Honnery D. Heat release model for the combustion of diesel oil emulsions in di diesel engines. Appl Thermal Eng 2005;25(14–15):2072–85. https://doi.org/10.1016/j.applthermaleng.2005.01.016.
[30] Stanton DW, Ray L, Buckendale Lecture 2013–01-2421 2013.
[31] Charlton SJ, Developing diesel engines to meet ultra-low emission standards, SAE Technical Papers doi:10.4271/2005-01-3628.
[32] Lucchini T, Della Torre A, D'Errico G, Montenegro G, Fiocco M, Maghbouli A. Automatic Mesh Generation for CFD Simulations of Direct-Injection Engines. SAE Technical Paper Series 2015. https://doi.org/10.4271/2015-01-0376.
[33] Kösters A, Karlsson A. Validation of the VSB2 spray model against spray A and spray H. Atom Sprays 2016;26(8):775–98. https://doi.org/10.1615/AtomizSpr.2015011670.
[34] Borg A, Lehtiniemi H, Mauss F, Private Communication, LOGE AB.
[35] Matrisciano A, Netzer C, Werner A, Borg A, Seidel L, Mauss F, A Computationally Efficient Progress Variable Approach for In-Cylinder Combustion and Emissions Simulations, in: SAE Technical Paper, SAE International, 2019. doi:10.4271/2019-24-0011.
[36] Dec JE, A conceptual model of di diesel combustion based on laser-sheet imaging, SAE Technical Papers (412).doi:10.4271/970873.
[37] Eismark J, Balthasar M, Karlsson A, Benham T, Christensen M, Denbratt I, Role of late soot oxidation for low emission combustion in a diffusion-controlled, High-EGR, heavy duty diesel engine, SAE Technical Papers 4970 (2009) 1–15. doi:10.4271/2009-01-2813.
[38] Eismark J, The role of piston bowl shape in controlling soot emissions from heavy-duty diesel engines., Doktorsavhandlingar vid Chalmers tekniska högskola. Ny serie: 4470, Chalmers University of Technology, 2018.
[39] Jung HH, Shelby MH, Newman CE, Stein RA. Effect of ethanol on part load thermal efficiency and CO2 emissions of SI engines. SAE Int J Eng 2013;6(1):456–69. https://doi.org/10.4271/2013-01-1634.
[40] Zeldovich J. The Oxidation of Nitrogen in Combustion and Explosions. Acta Physicochimica URSS 1946;21(4):218. https://doi.org/10.1515/9781400862979.364.
[41] Salehian A, Shirneshan A. The Effect of Cordierite-Platinum SCR Catalyst on the NOx Removal Efficiency in an Engine Fueled with Diesel-Ethanol-Biodiesel Blends. Catalysis Letters 2020;150(8):2236–53. https://doi.org/10.1007/s10562-020-03138-7.